Cement and Concrete Research 40 (2010) 687–698

Contents lists available at ScienceDirect

Cement and Concrete Research

journal homepage: http://ees.elsevier.com/CEMCON/default.asp

A novel two-dimensional method to measure surface shrinkage in cementitious materials

T.C. Chen [a,*], C.C. Ferraro [b], W.Q. Yin [a], C.A. Ishee [c], P.G. Ifju [a,*]

[a] University of Florida, Department of Mechanical and Aerospace Engineering, Gainesville, FL 32611-6250, United States
[b] University of Florida, Department of Civil and Coastal Engineering, Gainesville, FL 32611-6250, United States
[c] Florida Department of Transportation, State Materials Office, Gainesville, FL 32609, United States

ARTICLE INFO

Article history:
Received 10 April 2009
Accepted 26 November 2009

Keywords:
Shrinkage
Diffraction grating
Moire interferometry
Moisture diffusion

ABSTRACT

A novel experimental technique, Cure Reference Method (CRM), was developed for the measurement of surface shrinkage in cementitious materials. The technique combines the replication of diffraction grating on a specimen during the curing process and the use of high-sensitivity moiré interferometry. Once demolded, the specimen was stored in an environmental chamber in order to establish specific curing conditions. Measurements were conducted on a daily basis for the duration of 7 days by recording a set of the consecutive phase shifted fringe patterns using the Portable Engineering Moiré interferometer II (PEMI II). An automated fringe analysis system was developed and used to obtain displacement and strain information in two dimenzsions. Surface shrinkage behavior in both cement paste and mortar specimens was investigated by the use of the technique under controlled temperature and humidity conditions. Furthermore, an experimental control was developed in an effort to remove the effects of drying shrinkage on cementitious specimens at early ages. This was done in an effort to explore the relative contribution of autogenous shrinkage to the overall shrinkage in cementitious materials.

1. Introduction

Concrete experiences volume change during its service life, especially at early ages. Shrinkage development in concrete materials is a volumetric change. The combination of shrinkage and restraint contribute to the development of tensile stress and can subsequently cause cracking. Thus, the characterization of the surface shrinkage behavior in cementitious materials is important with regard to all the aspects of concrete design, such as the design of slabs, pavements and decorative concrete. Typically, the major contribution of total shrinkage is a result of drying shrinkage due to moisture diffusion and autogenous shrinkage due to hydration process between water and cement [1]. Thus, there are several factors which influence the shrinkage of cementitious materials, such as water/cement (w/c) ratio, surrounding drying condition/humidity, aggregate ratio (sand/cement = s/c), the geometry of the specimen and time [2–11].

Some experimental techniques have been used to measure the development of early-age shrinkage in cementitious materials. ASTM C157 is the standardized test method for the measurement of length change of cements and mortar specimens [12,13]. However, this method measures the average linear shrinkage. Embedded sensors, such as embedded strain gauges and fiber optics, are also popular for the measurement of shrinkage [14–16]. These methods provide point-measurements and the gathered information can be altered by the intrusive nature of these tests. There is little research available with regard to the two-dimensional measurement of surface shrinkage in cementitious materials. An optical technique called the digital photogrammetric method has been applied to measure the shrinkage on a full-field basis [17]. Nevertheless, it does not provide high sensitivity of strain measurement. Therefore, a two-dimensional, nonintrusive and high-sensitivity experimental technique for the measurement of time-dependent surface shrinkage in cementitious materials would be an alternative to methods currently available. Moiré interferometry is capable of measuring the relative displacement on the surface of cementitious specimen with an accuracy of 0.417 μm/fringe.

Originally, the Cure Reference Method (CRM) was developed for the measurement of residual strains that evolve in composite materials [18–22]. The method has also been applied to the measurement of post-gel chemical shrinkage of epoxies [23]. This paper details the methodology of CRM for the surface shrinkage measurement in cementitious materials. The CRM technique is nondestructive in nature and measures strain in two dimensions with a high degree of sensitivity. The method can be applied to the measurement of time-dependent surface shrinkage because the specimen measuring technique utilizes a diffraction grating which does not degrade over time. Some examples of the results obtained by

* Corresponding authors. Tel.: +1 3105006845.
E-mail address: jimchen@ufl.edu (T.C. Chen).

0008-8846/$ – see front matter © 2009 Elsevier Ltd. All rights reserved.
doi:10.1016/j.cemconres.2009.11.013

the moiré interferometry fringe patterns are presented herein. The automated fringe analysis system used to investigate the surface shrinkage behavior in both cement paste and mortar specimens is discussed. In an effort to measure autogenous shrinkage due to hydration, specimens were sealed to prevent the escape of moisture.

2. Experimental procedure

To better understand the details of the CRM experimental technique, a brief summary of the procedure is provided. The first step in this technique is to replicate the diffraction grating from a master grating substrate to the surface of the cementitious specimen after placement. The deformation of the specimen in the fluid state is not measured in CRM. However, the volume change of cementitious systems prior to setting is of little significance to inducing cracks. After the cementitious specimen becomes elastic (after setting), stresses can evolve within due to the constraining force provided from the rigid substrate. At this point in time, the in-plane dimensions of the specimen and the frequency of the grating on its surface remain the same. Immediately after the specimen is separated from the rigid substrate, the accumulated stress is released and the diffraction grating and the specimen are deformed. The change in the grating frequency captures the in-plane deformation of the specimen remarkable precision and accuracy. As desiccation occurs, the grating records the deformation on the surface of the specimen over time. The grating acts as an absolute reference to the stress-free state.

2.1. Replication of grating

The procedure for the grating replication is described herein is illustrated in Fig. 1. Typically, the diffraction grating has a frequency of 1200 lines/mm.

Step 1 A 57.1 mm × 57.1 mm silicone rubber RTV 6428 grating (master grating) is prepared by the replication from a photo resistant diffraction grating. Envirotex Lite epoxy is mixed, degassed, and added to master grating. Prior to placement, the epoxy is mixed and set cures for 2 h at room temperature (23 °C) to increase viscosity.

Step 2 A clean glass plate is then placed onto the pool epoxy in an effort to make it as thin as possible. The glass plate is then carefully removed horizontally from the master grating to prevent beads. Typically, the resultant thickness of epoxy layer is approximately 100 μm. Due to the relative thickness and compliance after cure, the epoxy is considered to provide a negligible amount of bonding to the cementitious specimen.

Step 3 A mold made of GE RTV 627 silicone rubber with an inner diameter of 28 mm and 11 mm in thickness is placed on to the master grating. After mixing, the cementitious fluid is poured into the mold and left to set for 24 h.

Step 4 The cementitious specimen is then demolded and separated from the master grating. Due to the lower bonding strength between the epoxy layer and the master grating, the epoxy diffraction grating is transferred onto the cementitious specimen.

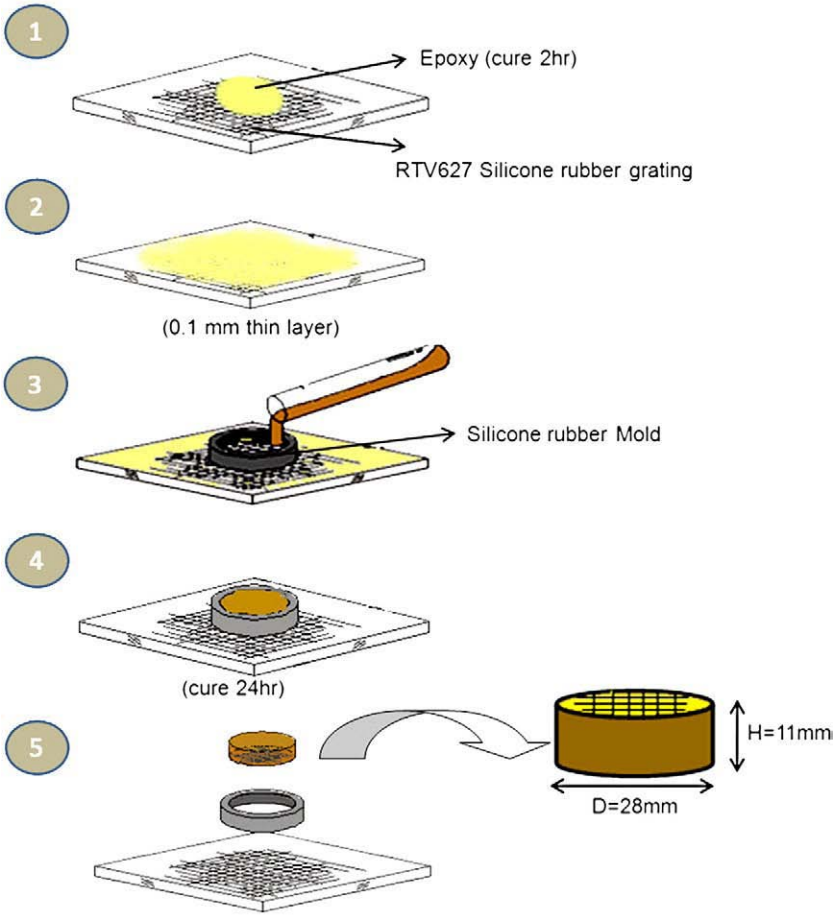

Fig. 1. Procedure of diffraction grating replication.

2.2. Environmental chamber setup

In this experiment, a 10×10×15 cm airtight storage container served as the environmental chamber. Sufficient desiccates were inserted into the chamber to create 0–2% relative humidity (RH) inside of the chamber. Conversely, 100%RH environment was created by replacing the desiccates with water. To create an environment with an RH50%, potassium carbonate saturated salt solutions were used. The laboratory temperature was standard room temperature of 23 °C. A temperature chamber was used to establish higher and lower temperatures such as 5 °C and 40 °C.

2.3. Equipment

The equipment used for the experiment shown in Fig. 2 is the Second Generation Portable Engineering Moiré interferometer (PEMI II). The operation of the high resolution digital camera and the fringe shifting control is managed by computer software. Typically, a set of 4 images is captured for the creation of a consecutive phase shifted fringe pattern. The strain resolution obtained from this equipment is approximately 50–100 με.

2.4. Moiré interferometry surface shrinkage measurement

The CRM experimental technique applied moiré interferometry [24] to measure the development surface shrinkage in cementitious materials. Moiré interferometry is an optical technique to record two-dimensional in-plane deformation information as interference fringe patterns or contour maps of U (horizontal) and V (vertical) displacement fields. The strains on the surface of the specimens were determined from the displacement fields using the following strain displacement relationships, where is N fringe order, f is two times the frequency of the diffraction grating, and Δx or Δy is the selected gauge length:

$$\varepsilon_x = \frac{\partial U}{\partial x} \approx \frac{1}{f}\left[\frac{\Delta N_x}{\Delta x}\right] \tag{1}$$

$$\varepsilon_y = \frac{\partial V}{\partial x} \approx \frac{1}{f}\left[\frac{\Delta N_y}{\Delta y}\right] \tag{2}$$

$$\varepsilon_{xy} = \frac{\partial U}{\partial y} + \frac{\partial V}{\partial x} \approx \frac{1}{2f}\left[\frac{\Delta N_x}{\Delta y} + \frac{\Delta N_y}{\Delta x}\right] \tag{3}$$

For the measurement of shrinkage in cementitious materials, the master grating was positioned in the moiré interferometer as the reference grating for the tuning of the moiré interferometer to a null field which is regarded as the absolute reference of non-deformation. By replacing the master grating with the cementitious specimen, the initial (day 1) fringe patterns are captured by the digital camera. Subsequent to image capture, the specimen was stored in the chamber which provided a specific environment for six days. Once every 24 h the specimen was removed from the chamber and positioned in the moiré interferometer, a set of the consecutive phase shifted moiré fringe patterns was recorded. The specimen was returned to the environmental chamber after completion of the measurement. An automated strain analysis system based on phase shifting theory [25–27] was developed to obtain the two-dimensional displacement and strain maps for the measurements from day 1 to day 7. Shrinkage as a function of time and location was determined accordingly.

3. Results and discussion

For this research, the measurement of shrinkage on the unsealed cement paste and mortar specimens was performed. However, some of the specimens were completely sealed in an effort to measure autogenous shrinkage of cementitious systems. In the tests, 1000×1000 pixel U and V-field moiré interferometry fringe patterns were recorded on a daily basis for 7 days.

3.1. Unsealed cement paste specimens

The cement paste specimens were made with 0.5 w/c using ASTM C150 Type I Portland cement. Tests were performed for specimens exposed to different combinations of environmental temperature and humidity.

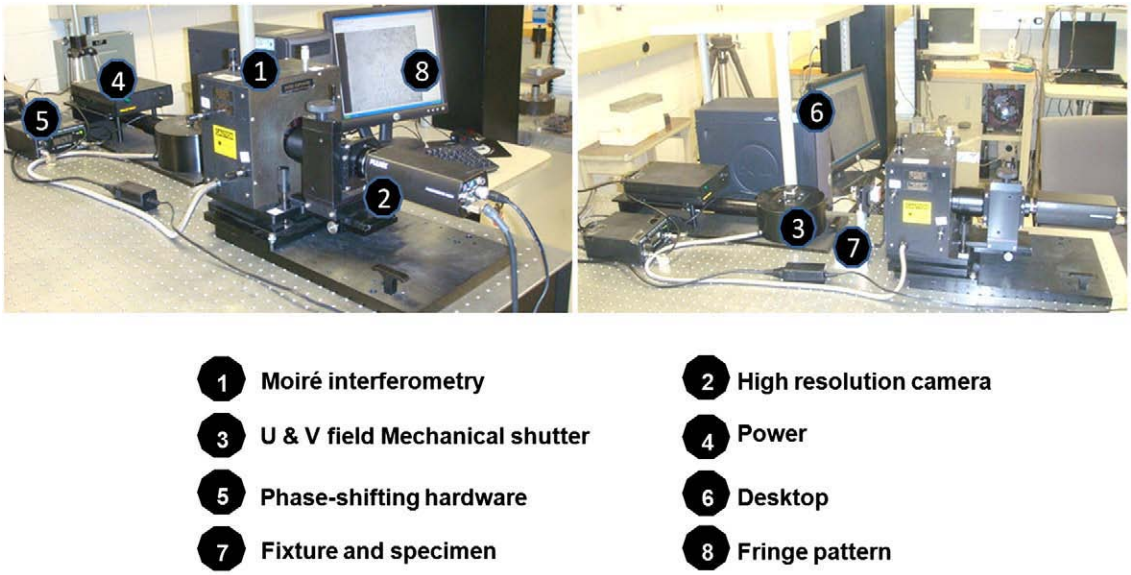

Fig. 2. Experimental setup PEMI II.

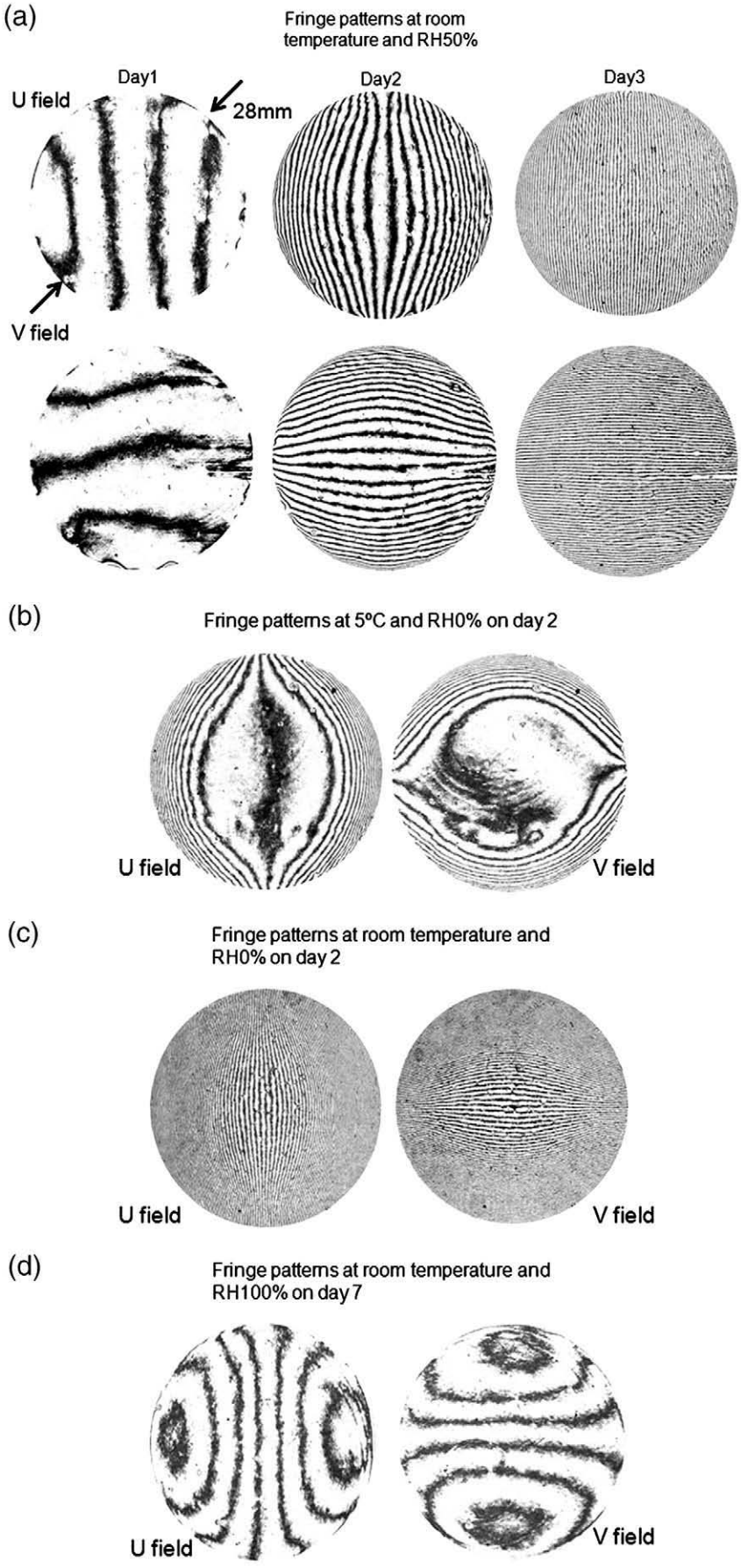

Fig. 3. Moiré interferometry fringe patterns for unsealed cement paste specimens at different drying conditions.

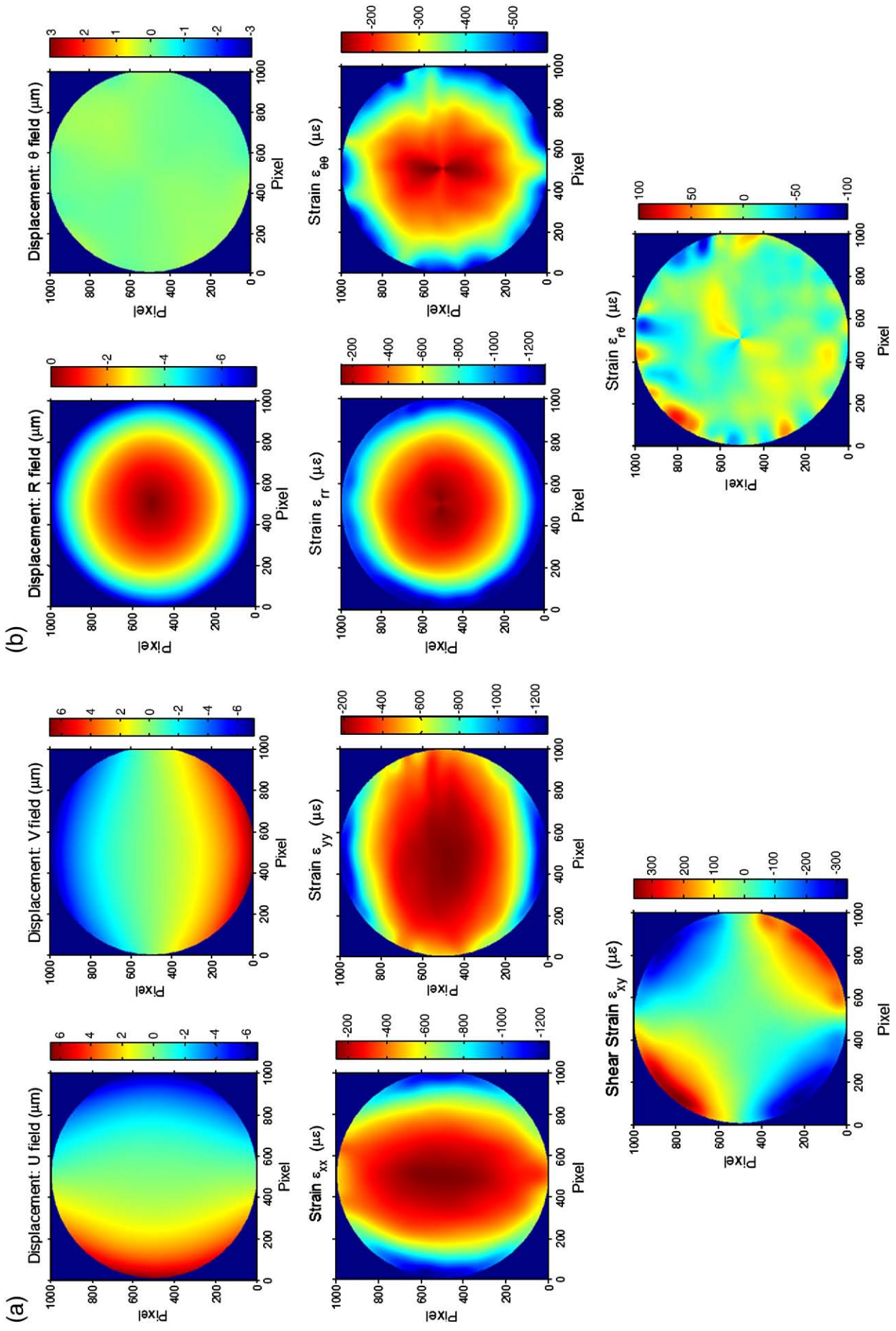

Fig. 4. Full-field information in both (a) *x*–*y* and (b) polar coordinates on day 2 at room temperature and RH50%.

Fig. 3(a) shows the *U* and *V*-field moiré interferometry fringe patterns for the cement paste specimens at room temperature and RH50% from day 1 to day 3. Both fields have similar fringe distributions due to axisymmetric conditions. And, the number of fringes increases with time and the fringe density is higher near the outer surface than in the inner core. The concept that shrinkage is larger near the edges of a cementitious specimen is consistent with reported values from literature [28]. The initial fringe patterns (day 1) revealed a local expansion or a potential swelling effect after the specimen was demolded, but this was not significant.

Fig. 3(b) and (c) show the fringe patterns for specimens stored at 5 °C and room temperature respectively at RH0% on day 2. The results indicate that the curing temperature is an influential factor to the fringe distributions. This phenomenon is a result of the temperature dependent rate of hydration of the cement paste. Higher curing temperatures will result in larger rates of hydration [28] which, contribute to the larger fringe patterns observed for specimens exposed to higher curing temperatures for specimens which are the same age. As observed with the other specimens, the fringe density was higher near the outer surface as the examples shown in Fig. 3(a). This phenomenon is due to a higher degree of shrinkage measured at the outer surface.

Fig. 3(d) shows the fringe patterns at room temperature and RH100% on day 7. Compared with specimens exposed to RH less than 100%, this specimen has fewer fringes in both fields. This phenomenon is due to the lack of relative surface shrinkage due to dehydration of the specimen. The fringes curve outwardly as a result of the nature of the measuring technique and there are enclosed fringes close to the outer surface, which are a result of a relatively large amount of localized surface shrinkage.

The two-dimensional maps for each day were obtained via the automated fringe analysis system. Here, only the two-dimensional information at room temperature and RH50% on day 2 is shown as Fig. 4(a) in *x*–*y* coordinates. The surface shrinkage measurements are converted to polar coordinates and presented in Fig. 4(b).

The displacement maps in both coordinate systems indicate that the specimen experienced surface shrinkage. The fact that the surface shrinkage is larger near the outer surface was found from the normal strain maps in both coordinate systems, which again is consistent with literature and previous results presented herein.

The shear strain map in *x*–*y* coordinate shows the maximum shear strain occurred at four locations, which were on the outer surface in ± 45 and $\pm 135°$ directions. The shear stain was approximately zero along the vertical and horizontal center lines. A likely explanation can be attributed to the use of the Mohr circle. In polar coordinates, the theoretical angular displacement and shear strain equal zero due to axisymmetry. However, the results show these two maps are not uniform due to the noise in the analysis. However, the displacement and strain values in this direction are insignificant compared with the other fields.

The strain analysis for the *U*-field fringe pattern at room temperature and RH100% on day 7 is shown in Fig. 5. Globally, the specimen experienced shrinkage from the *U*-field displacement information. Locally, swelling occurred in the area near the outer surface due to moisture gain; the inner area still experienced the some localized autogenous shrinkage due to hydration. The locations of zero shrinkage approximately correspond to the centers of the enclosed fringes.

Fig. 6 shows the surface shrinkage, which here was defined as the value of radial strain, measured from the center of the specimen (position = 0) to the outer surface for specimens exposed to different humidity conditions. Surface shrinkage increased with time and larger shrinkage occurred in the area close to the outer surface. The results are consistent with the notion that the rate of shrinkage will be larger in localized regions of the cementitious volume which are adjacent to the exposed surface.

Fig. 7 presents the results with respect to relative humidity and temperature effects on the average surface shrinkage of cement pastes over time. The average surface shrinkage is defined as the diameter change of the specimen divided by the original diameter. It was derived using Eq. (1) with the gauge length of 28 mm along the horizontal centerline in the *U*-field fringe pattern or using Eq. (2) with

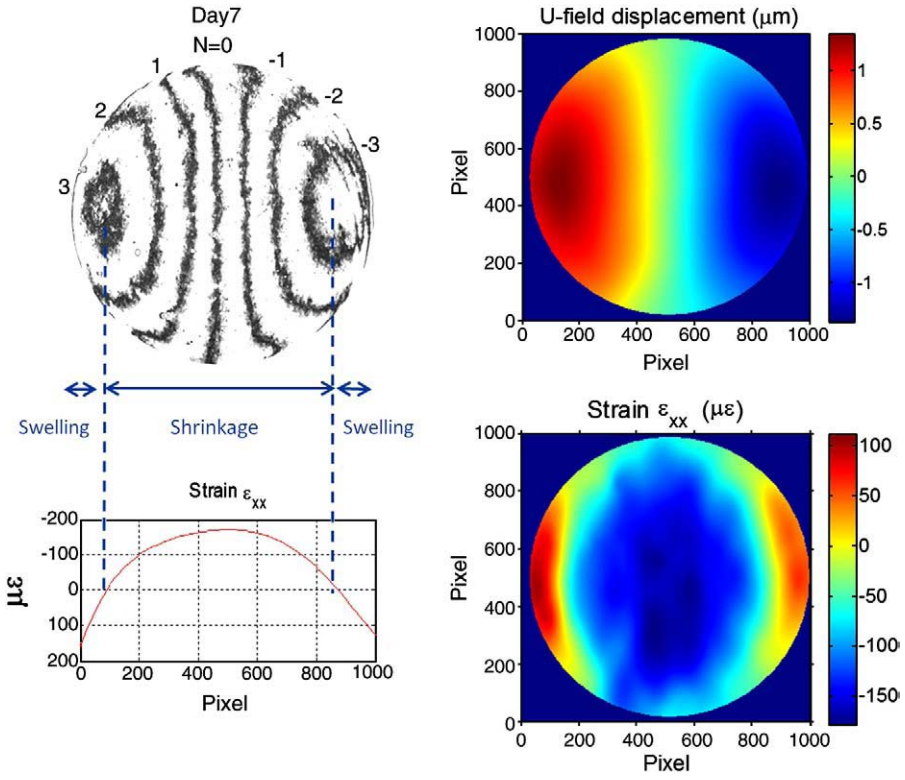

Fig. 5. The strain analysis for *U*-field fringe pattern at RH100% and room temperature on day 7.

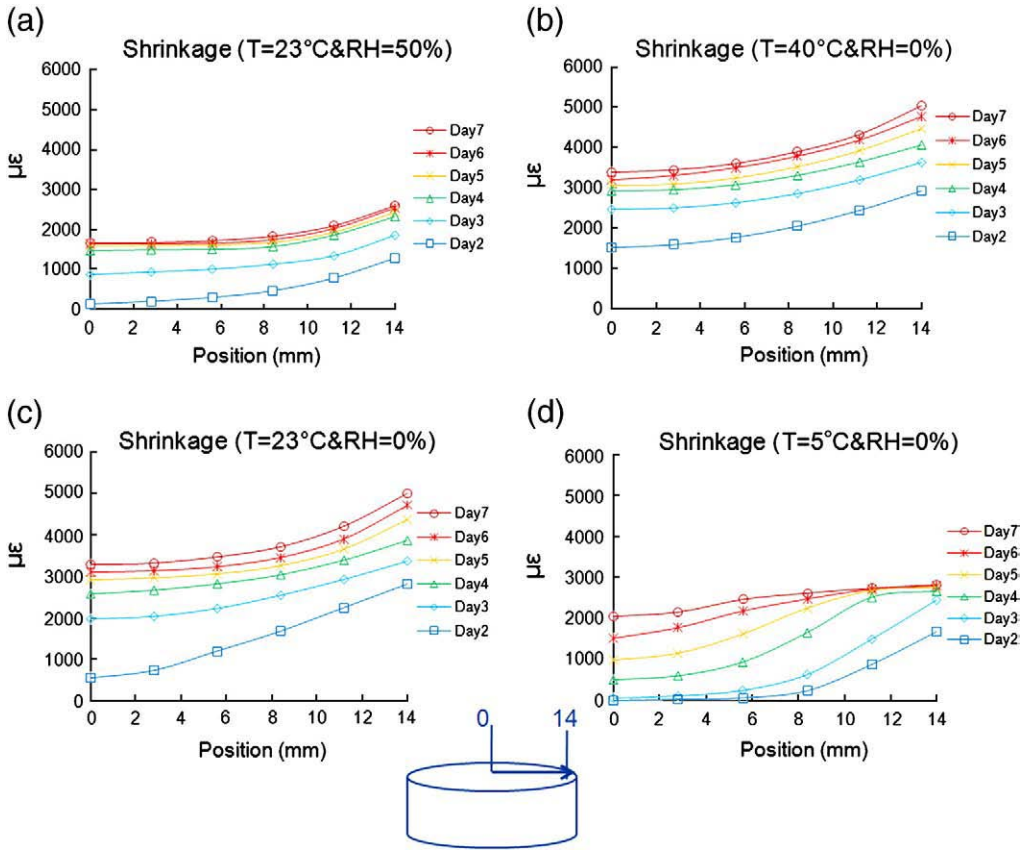

Fig. 6. Surface shrinkage measurements from center to outer surface at different drying conditions.

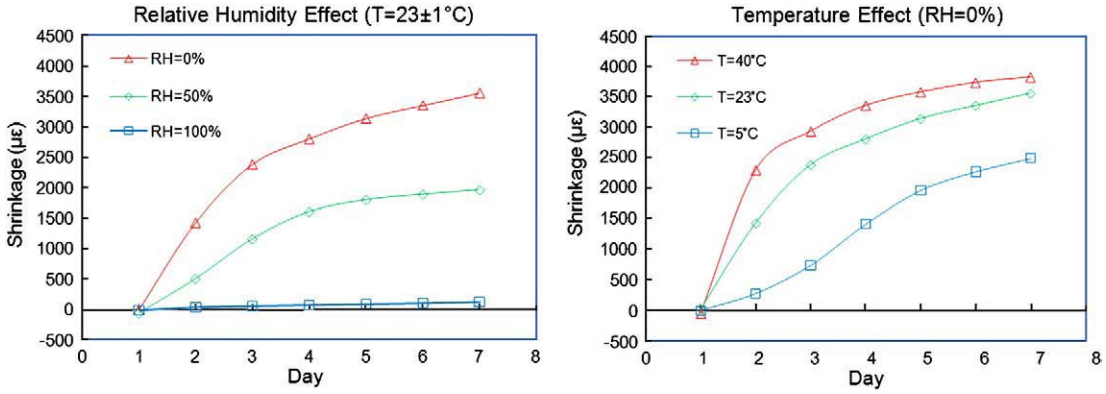

Fig. 7. Relative humidity and temperature effects on the average surface shrinkage for unsealed cement paste specimens.

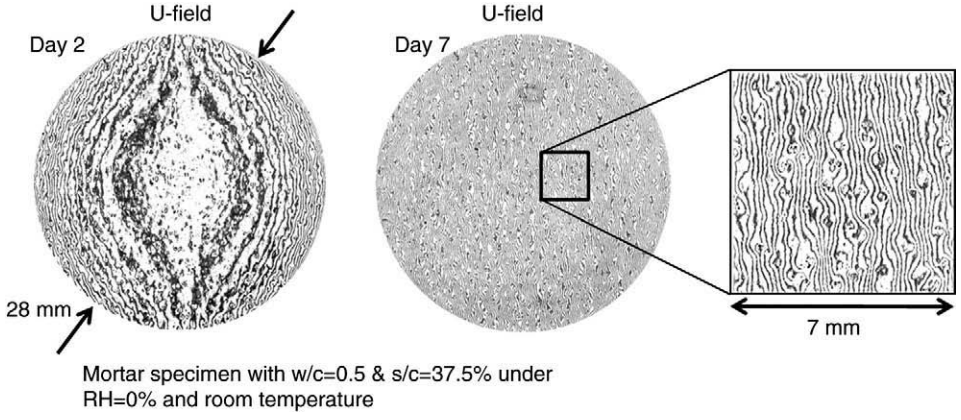

Fig. 8. *U*-field moiré fringe patterns for mortar with *s*/*c* ratio = 37.5%.

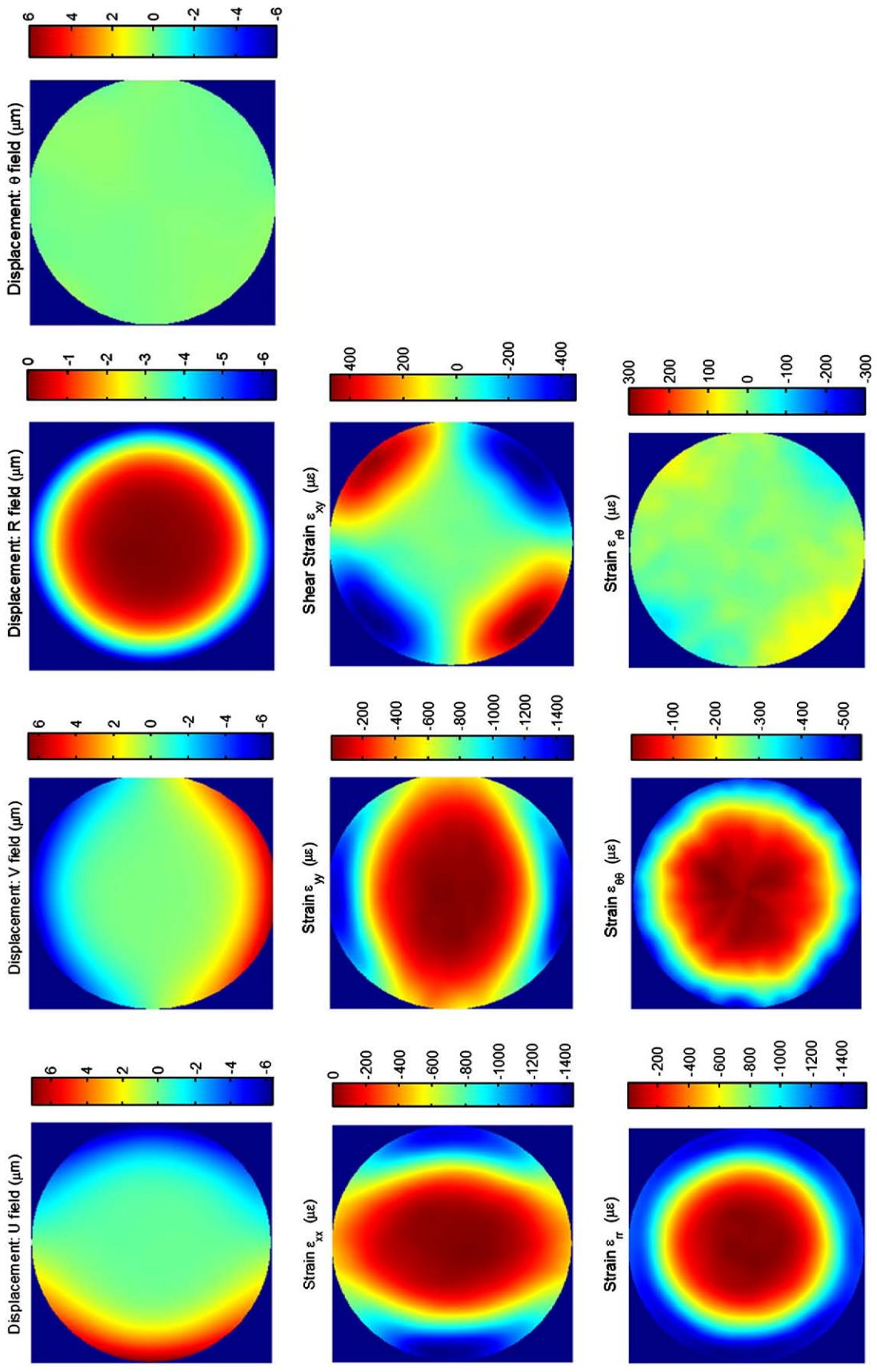

Fig. 9. Full-field displacement and strain information for mortar with $s/c = 37.5\%$ on day 2.

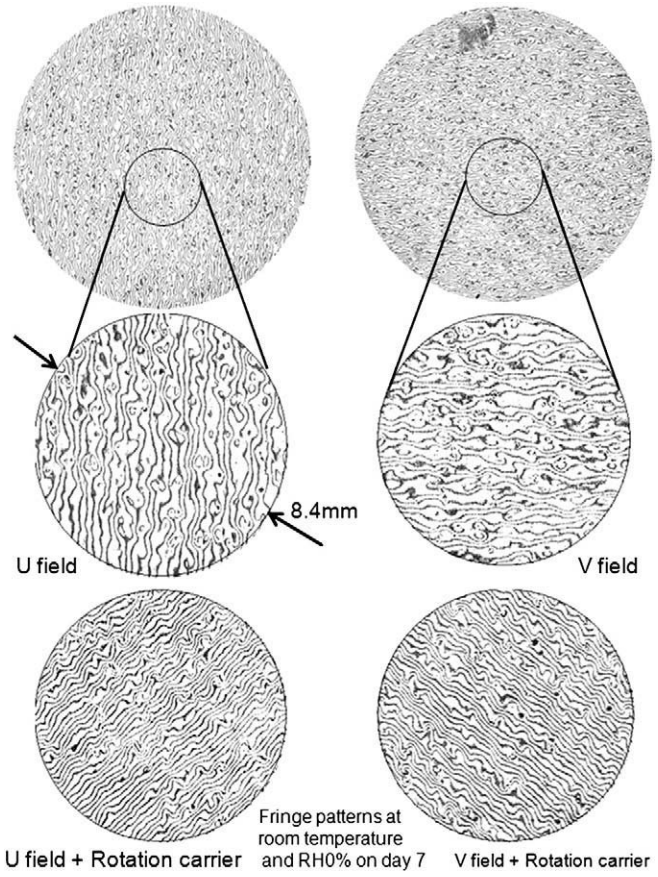

Fig. 10. Moiré interferometry fringe patterns, their insets, and the insets with rotation carriers for the mortar specimen with $s/c = 75\%$ at room temperature and RH0% on day 7.

the gauge length of 28 mm along the vertical centerline in the *V*-field fringe pattern.

3.2. Unsealed mortar specimens

The mortar specimens were made by mixing ASTM C778 sand with cement and water ($w/c = 0.5$). The fringe patterns for the specimen with sand/cement ratio (s/c) = 37.5% at RH0% and room temperature are shown in Fig. 8. *V*-field fringe patterns are not presented here due to symmetry with the *U* field which was established earlier within this text. The inset reveals the fringes were affected by the existence of the sand particles. Sand lowers the fringe density locally. However, the counting of the number of fringes manually was used to determine the average surface shrinkage of the specimen.

The displacement and strain analysis for day 2 fringe patterns is presented in Fig. 9. The maps are relatively smooth which does not reflect the actual strain information due to an averaging effect. However, it is still acceptable and reasonable for the measurement of the distribution of the strain to be measured globally. As observed with the cement paste specimens, the surface shrinkage is larger in the area close to the outer surface than in the inner core.

Fig. 10 shows the fringe patterns, the insets, and the insets with carrier fringes of rotation for the mortar specimen with $s/c = 75\%$ at room temperature and RH0% on day 7.

The inset reveals counting fringes is challenging due to the irregularity and distortion of fringe patterns. However, carrier fringes of rotation make it possible to count the number of fringes for the determination of a value for the average surface shrinkage. Carrier fringes of rotation can be introduced into moiré fringe patterns by rotating moiré interferometer with respect to the specimen.

The use of the superposed fringe patterns in the analysis does not change the two-dimensional strain information. Theoretically, the two-dimensional strain maps can be obtained with any size of gauge length via the automatic fringe analysis system. However, in the event the selected gauge length is too large, the resultant maps would not reflect local information due to an averaging effect. Thus, the maps would appear to be too smooth, with an apparent lack of localized

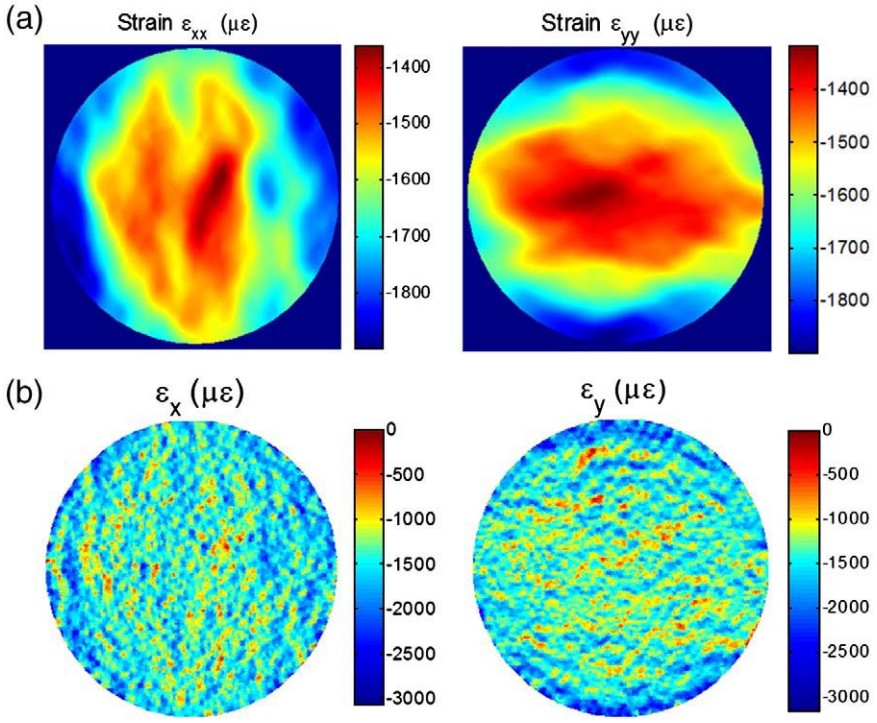

Fig. 11. Strain analysis with (a) large gauge length and (b) small gauge length for the mortar specimen with $s/c = 75\%$ at room temperature and RH0% on day 7.

fringe patterns. Day 7 moiré fringe patterns were analyzed with both small and large gauge lengths. Fig. 11 illustrates the difference in that gauge length size has on the resultant fringe patterns. The strain information with small gauge length might display the strain distribution more properly. Consistent with the previous results presented herein, larger surface shrinkage was measured in the area near the outer surface. From Fig. 11(b), the surface shrinkage of mortar specimens was lower compared to cement specimens due to the existence of the distributed sand within the mix.

Fig. 12 shows both fine aggregate quantity and RH effects on the average surface shrinkage of mortar specimens. The results clearly indicate that mortar specimens which have a larger quantity of sand, have a lower average surface shrinkage which is consistent with results reported in literature [28]. Also, the average surface shrinkage increases with a decrease in relative humidity.

3.3. Sealed cement paste specimens

In an effort to investigate the component of autogenous surface shrinkage with respect to the overall shrinkage, the entire cementitious specimen was sealed with aluminum sheets and then wrapped with plastic wrap Instead of being stored in the chamber. This was done to prevent the exchange of moisture with the surrounding environment and to remove the effect of surface drying shrinkage. Once a day the specimen was unsealed, a measurement was taken as quickly as possible and then the specimen was resealed after testing. Fig. 13 shows the fringe patterns for $w/c = 0.4$ & 0.6 at room temperature on day 7.

The results indicate that the fringes are quite uniformly spaced at both the center and near the outer surface. Unlike the results for the specimens which were obtained for the unsealed specimens, the sealed specimens do not experience differential surface shrinkage. These results indicate that the surface shrinkage effects due to drying shrinkage did not take place for these specimens and the measured surface shrinkage was primarily due to autogenous shrinkage as a result of hydration. Fig. 13 indicates that the number of fringes developed by the specimen with a w/c of 0.4 is greater than those developed in the specimen with w/c of 0.6 This phenomenon is due to the differences in hydration rate of cementitious specimens with different w/c, where lower w/c specimens hydrate and experience shrinkage at a faster rate [29]. The U-field fringe pattern on day 7 is shown in Fig. 14.

The strain maps obtained through the automated fringe analysis were not uniform due to systemic noise. However, the U-field strain map results indicate that the strain is uniform over the entire field subsequent to the enlargement of the scale. By obtaining displacement fields and plotting the displacement distribution along the horizontal axis, the results indicate that the slope is very close to constant, which indicates the surface strain is uniform. Both w/c ratio and temperature effects on surface autogenous shrinkage were investigated and the results are presented in Fig. 15. The results illustrate that autogenous shrinkage increased with decreased w/c ratio and with increased temperature at early ages.

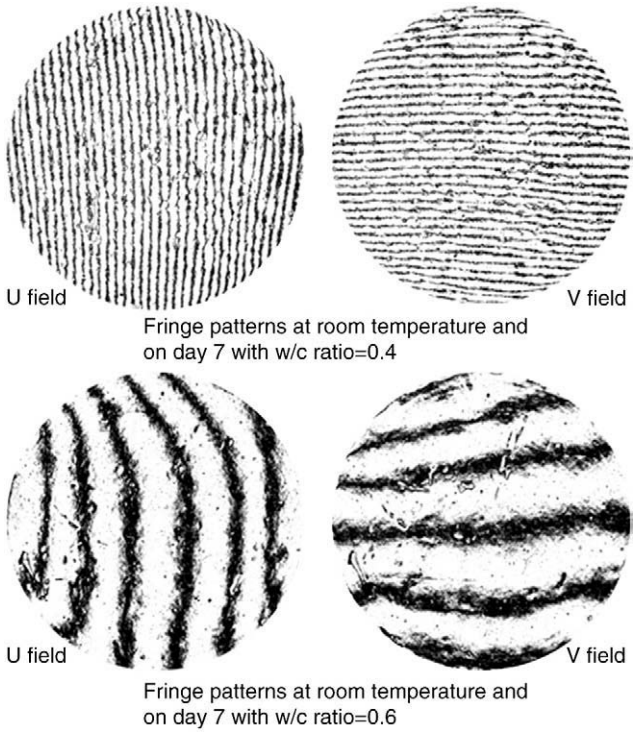

Fig. 13. Moiré interferometry fringe patterns for sealed cement paste specimens.

4. Conclusions

The experimental technique for the measurements of shrinkage in concrete materials has been developed based on the Cure Reference Method and high-sensitivity moiré interferometry. An automated strain analysis system was developed and applied to obtain the two-dimensional displacement and strain maps in both x–y and polar coordinates. This technique measures the changes to the surface of cementitious which is different than the measurement of volumetric changes. However, the technique provides a highly-sensitive/highly-accurate system for the measurement of surface changes in cementitious materials. The technique provides an accurate measurement of autogenous shrinkage of cementitious materials. The experimental results have shown that the shrinkage behavior of cement pastes and mortars had agreement with that documented in

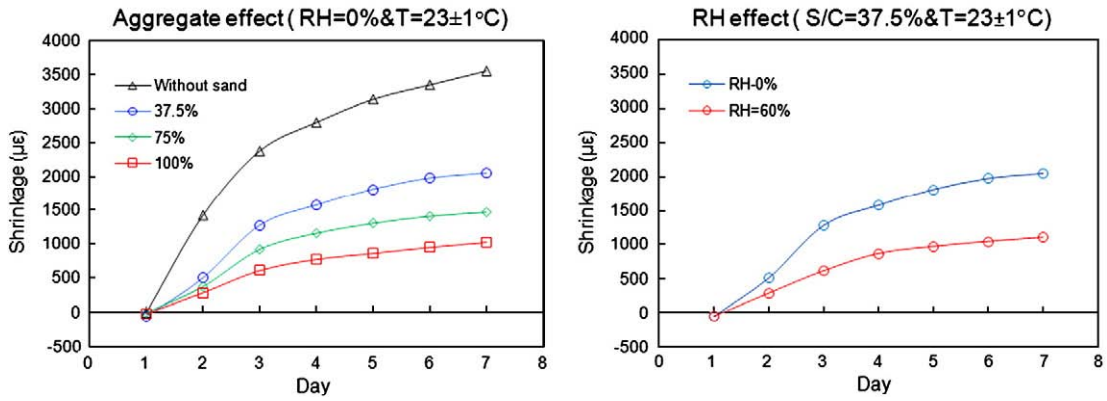

Fig. 12. Aggregate and relative humidity effects on the average surface shrinkage for unsealed mortar specimens.

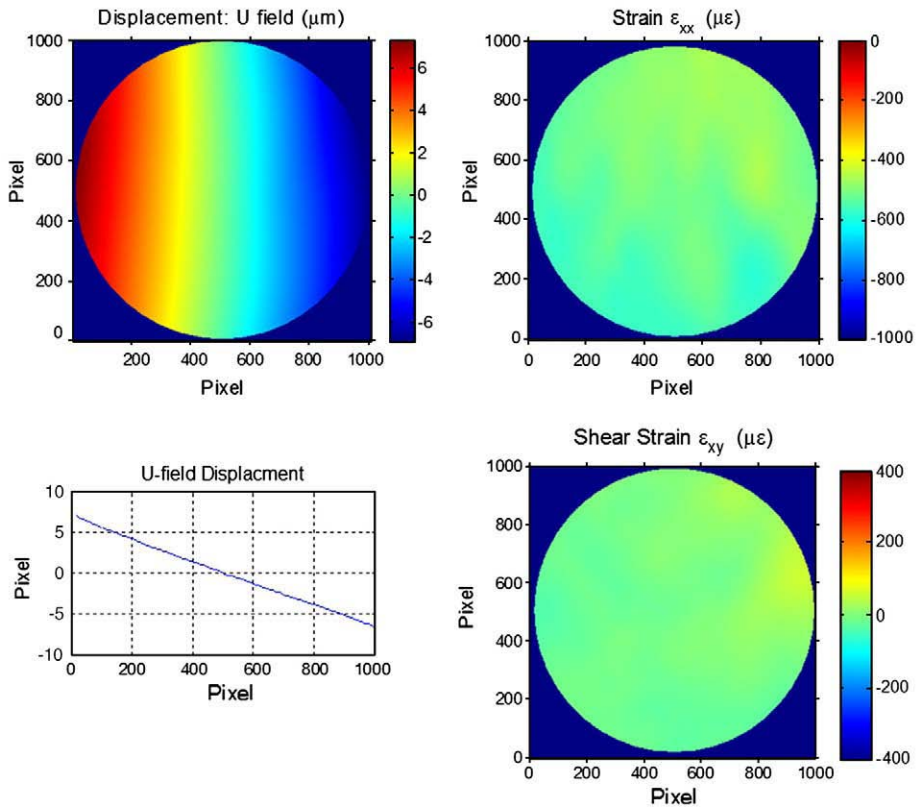

Fig. 14. Analysis for the sealed cement paste specimen with $w/c = 0.4$ at room temperature on day 7.

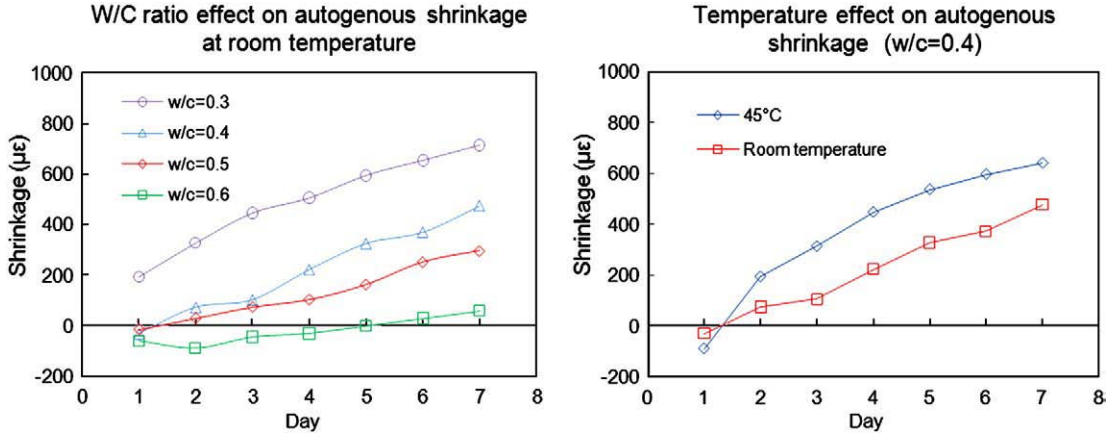

Fig. 15. Autogenous surface shrinkage results with various w/c and temperatures.

literature. The experimental data can be used in numerical model to determine the material property of shrinkage.

5. Limitations

This technique measures the surface displacements of cementitious materials, and the results differ from the actual strain distribution of natural cementitious materials.

Therefore, the technique does not capture the total volume change of that occurs within a cementitious system, nor can it account for moisture gradients that occur across the depth of the sample. Since moiré interferometry is limited to the measurement of deformation of a maximum area of around 35 mm in diameter, lager samples cannot be tested. However, further research and potential application of this method should include the creation of a Finite Element model which can be used to predict shrinkage in larger cementitious specimens after surface shrinkage properties are determined. Furthermore, the use of an epoxy bonding system adds a degree of uncertainty to the nature of the surface displacement measurements. Differential moisture gradients and contributions to tensile restraint are two potential effects that have not yet been accounted for per this testing method.

Acknowledgements

The authors are grateful to the Florida Department of Transportation (FDOT) State Materials Office for the financial support and to the reviewers for their valuable comments.

References

[1] S. Mindess, J. Francis Young, D. Darwin, Concrete, Second editionPrentice Hall, New Jersey, 2003.
[2] ACI 209.1R-05 Report on Factors Affecting Shrinkage and Creep of Hardened Concrete.
[3] B. Bissonnette, P. Pierre, M. Pigeon, Influence of key parameters on drying shrinkage of cementitious materials, Cement and Concrete Research 29 (1999) 1655-1622.
[4] S.A. Al-Saleh, R.Z. Al-Zaid, Effects of drying conditions, admixtures and specimen size on shrinkage strains, Cement and Concrete Research 36 (2006) 1985–1991.
[5] M.H. Zhang, C.T. Tam, M.P. Leow, Effect of water-to-cementitious materials ratio and silica fume on the autogenous shrinkage of concrete, Cement and Concrete Research 33 (10) (2003) 1687–1694.
[6] B. Veronique, M. Pierre, K. Abdelhafid, L. Ahmed, R. Noureddine, Autogenous deformations of cement pastes: part II. W/C effects, micro–macro correlations, and threshold values, Cement and Concrete Research 36 (1) (2006) 123–136.
[7] M. Pierre, B. Veronique, L. Ahmed, K. Abdelhafid, Autogenous deformations of cement pastes: part I. Temperature effects at early age and micro–macro correlations, Cement and Concrete Research 36 (1) (2006) 110–122.
[8] K. Kohno, T. Okamoto, Y. Isikawa, T. Sibata, H. Mori, Effects of artificial lightweight aggregate on autogenous shrinkage of concrete, Cement and Concrete Research 29 (4) (1999) 611–614.
[9] E. Tazawa, S. Miyazawa, Influence of constituents and composition on autogenous shrinkage cementitious materials, Magazine of Concrete Research 49 (178) (1997) 15–22.
[10] E. Tazawa, S. Miyazawa, Influence of cement and admixture on autogenous shrinkage of cement paste, Cement and Concrete Research 25 (2) (1995) 281–287.
[11] M.J. Millard, K.E. Kurtis, Effects of lithium nitrate admixture on early-age cement hydration, Cement and Concrete Research 38 (4) (2008) 500–510.
[12] ASTM C157/C157M-06 Standard Test Method for Length Change of Hardened Hydraulic-Cement Mortar and Concrete.
[13] D.W. Mokarem, R.E. Weyers, D.S. Lane, Development of a shrinkage performance specifications and prediction model analysis for supplemental cementitious material concrete mixtures, Cement and Concrete Research 35 (2005) 918–925.
[14] J.-K. Kim, C.-S. Lee, Prediction of drying shrinkage in concrete, Cement and Concrete Research 28 (1998) 985–994.
[15] Y. Yang, R. Sato, K. Kawai, Autogenous shrinkage of high strength concrete containing silica fume under drying at early ages, Cement and Concrete Research 35 (2005) 449–456.
[16] W.R. Habel, D. Hofmann, B. Hillemeier, Deformation measurements of mortars at early ages and of large concrete components on site by means of embedded fiber-optic microstrain sensors, Cement and Concrete Composites 19 (1997) 81–102.
[17] F. Yilmazturk, S. Kulur, B.Y. Pekmezci, Measurement of shrinkage in concrete samples using digital photogrammetric methods, The International Archives of the Photogrammetry, Remote Sensing and Spatial Information Sciences, Vol. 34, 2003, Part XXX.
[18] P.G. Ifju, J.E. Masters, W.C. Jackson, The use of moiré interferometry as an aid to standard test-method development for textile composite materials, Composites Science and Technology 53 (1995) 155–163.
[19] P.G. Ifju, B.C. Kilday, X. Niu, S.C. Liu, A novel method to measure residual stresses in laminated composites, Journal of Composite Materials 33 (16) (1999).
[20] P.G. Ifju, X. Niu, B.C. Kilday, S.-C. Liu, S.M. Ettinger, Residual strain measurement in composites using the cure-reference method, Journal of Experimental Mechanics 40 (2000) 22–30.
[21] N.M. Strickland, W. Yin, P.G. Ifju, Residual strain measurement analysis of woven composites using phase shifting, Proceedings of the 2007 SEM Conference on Experimental Mechanics, Springfield, MA, USA, June 4–6, 2007.
[22] G.P. Ifju, B.C. Kilday, X. Niu, S.C. Liu, Residual stress measurements in AS4/3501-6 laminates, Postconference Proceedings of SEM Spring Conference on Experimental Mechanics, Bellevue, WA, 1997, pp. 193–200.
[23] Shao-Chun Liu, “Residual Stress Characterization for Laminated Composites”, Ph. D. Dissertation, University of Florida, Gainesville, Florida (1999).
[24] D. Post, B. Han, P.G. Ifju, High Sensitivity Moiré: Experimental Analysis for Mechanics and Materials, Springer-Verlag, New York, 1994.
[25] J.M. Huntley, Automated fringe pattern analysis in experimental mechanics: a review, Journal of Strain Analysis 33 (2) (1998) 105–125.
[26] D.C. Ghiglia, M.D. Pritt, Two-Dimensional Phase Unwrapping: Theory, Algorithm, and Software, Wiley, New York, 1998.
[27] R.C. Gonzalez, R.E. Woods, S.L. Eddins, Digital Image Processing Using MATLAB, Prentice Hall, New York, 2003.
[28] A. Neville, Properties of Concrete4th ed, Pearson Education Limited, 1995.
[29] B. Persson, Experimental studies on shrinkage of high performance concrete, Cement and Concrete Research 28 (1998) 1023–1036.